https://doi.org/10.5194/egusphere-2025-978
Preprint. Discussion started: 21 March 2025

Evaluating the Utility of Sentinel-1 in a Data Assimilation System for Estimating Snow Depth in a Mountainous Basin

Bareera N. Mirza[1], Eric E. Small[2], Mark S. Raleigh[1]
[1]College of Earth, Ocean, and Atmospheric Sciences, Oregon State University, Corvallis, OR, USA
[2]Geological Sciences, University of Colorado, Boulder, CO, USA
Correspondence to: Bareera N. Mirza (mirzaba@oregonstate.edu)

Abstract:

Seasonal snow plays a critical role in hydrological and energy systems, yet its high spatial and temporal variability makes accurate characterization challenging. Historically, remote sensing has had limited success in mapping snow depth and snow water equivalent (SWE), particularly in global mountain areas. This study evaluates the temporal and spatial accuracy of recently developed snow depth retrievals from the Sentinel-1 (S1) C-band spaceborne radar and their utility within a data assimilation (DA) system for characterizing mountain snowpack. The DA framework integrates the ensemble-based Flexible Snow Model (FSM2) with a Particle Batch Smoother (PBS) to produce daily snow depth maps at a 500-meter resolution using S1 snow depth data. The S1 data were evaluated from 2017 to 2021 in and near the East River Basin, Colorado, using daily data at 12 ground-based stations for temporal evaluation and four LiDAR snow depth surveys from the Airborne Snow Observatory (ASO) for spatial evaluation. The analysis revealed significant inconsistencies in temporal and spatial errors of S1 snow depth, with higher spatial errors. Errors increased with time, especially during ablation periods, with an average temporal RMSE of 0.40 m. In contrast, the spatial RMSE exceeded 0.7 m, and S1 had poor spatial agreement with ASO LiDAR ($R^2 < 0.3$). Experiments with DA window sizes showed minimal performance differences for full-season and early-season windows. Joint assimilation of S1 snow depth with MODIS Snow Disappearance Date (SDD) yielded similar temporal errors in snow depth but degraded the performance in space relative to assimilating S1 alone. Assimilation of SDD alone outperformed S1 snow depth assimilation spatially, indicating that S1 has limited utility in a DA system. Future work should address retrieval biases, refine algorithms, and consider other snow datasets in the DA system to improve snow depth and SWE mapping in diverse snow environments globally.

https://doi.org/10.5194/egusphere-2025-978
Preprint. Discussion started: 21 March 2025

1. Introduction

Seasonal snow is a natural freshwater reservoir for around 20% of the world's population (Barnett et al., 2005) and plays a key role in the global energy budget. Global mapping of snow characteristics like snow water equivalent (SWE) is a critical challenge, especially in steep and complex mountain terrain where SWE has high spatial and temporal variability (Clark et al., 2011; Kinar and Pomeroy, 2015; López-Moreno et al., 2011; Raleigh and Small, 2017). The snow community has been developing ground measurement, modeling, and remote sensing techniques through campaigns (e.g., NASA SnowEx) to advance our capabilities for estimating snow characteristics. Despite these efforts, there is still no globally available snow dataset in mountainous terrain at appropriate resolutions (~100s m or finer). Where point SWE measurements exist (e.g., stations), the high spatiotemporal variability makes it challenging to extrapolate SWE across global mountain environments (Cluzet et al., 2022; Dozier, 2011; Dozier et al., 2016; Elder et al., 1998; Grünewald et al., 2010; Herbert et al., 2024; Molotch and Bales, 2006). Improving our ability to estimate SWE in complex mountain regions requires continued advancements in global snow measurement and modeling techniques.

Optical satellite remote sensing has been used extensively in estimating snow properties. Spaceborne photogrammetry is effective for retrieving high-resolution snow depth (Marti et al., 2016; McGrath et al., 2019). However, this estimation is unavailable during cloudy periods and in dense forests. Spaceborne laser altimetry, such as ICESat and ICESat-2 has demonstrated some capability in mapping snow depth (Besso et al., 2024; Deschamps-Berger et al., 2023; Hu et al., 2022; Treichler and Kääb, 2017), but errors are high and spatial-temporal sampling is sparse. Optical remote sensing techniques for snow cover area (SCA) mapping, using sensors like Landsat, MODIS, and Sentinel-2, permit monitoring snow cover extent (e.g., Stillinger et al., 2023). However, accurate mapping is hindered by cloud cover or dense vegetation (Aalstad et al., 2020). While optical remote sensing cannot measure SWE or snow depth, the information on SCA depletion can guide model-based estimates of SWE (e.g., Margulis et al., 2019; Rittger et al., 2016).

Passive microwave remote sensing retrievals have traditionally been used to retrieve snow depth (Foster et al., 1996; Kelly et al., 2003) and SWE (Chang et al., 1987; Derksen et al., 2005) however, its coarse spatial resolution (up to ~25km) cannot capture the variability of mountain snowpack,

https://doi.org/10.5194/egusphere-2025-978
Preprint. Discussion started: 21 March 2025

and its accuracy is reduced in wet or deep snow conditions (over 1m; Luojus et al., 2021). In contrast, active microwave remote sensing, such as Sentinel-1's (S1) C-band synthetic aperture radar (SAR) backscatter data, has shown potential in mapping mountain snow depth at a scale of 0.5 km or finer (Lievens et al., 2019). S1 data have the potential to improve understanding of mountain snow distributions and associated processes like orographic precipitation dynamics and streamflow generation (Brangers et al., 2024; Girotto et al., 2024). Nevertheless, S1 snow depth data has two fundamental challenges: (1) the data are not temporally continuous, and (2) snow density is required to convert snow depth to SWE (snow depth to SWE = density x snow depth). Two possible solutions are: (1) machine learning (Broxton et al., 2024, 2019; Dunmire et al., 2024) or (2) data assimilation (DA) frameworks (Smyth et al., 2022; Alonso-González et al., 2022). Machine learning has been used to produce temporally continuous snow depth data utilizing the S1 snow depth data (P. Broxton et al., 2024), but may require region-specific training due to geographic variations in snowpack characteristics, making it less suitable for global mapping. In contrast, the assimilation of remotely sensed snow depth can improve snowpack estimation (including estimates of snow density) and provide temporally continuous data (Deschamps-Berger et al., 2022; Girotto et al., 2020; Largeron et al., 2020; Margulis et al., 2015; Smyth et al., 2019, 2020) , yet DA remains an underexplored pathway for spatiotemporal SWE mapping with S1 snow depth.

While S1 snow depth data have the potential to guide DA systems to produce comprehensive spatiotemporal mountain SWE maps, there have been discrepancies in the reported spatial and temporal errors, which prompt questions about its reliability. Independent evaluations have reported large errors (Broxton et al., 2024; Dunmire et al., 2024; Hoppinen et al., 2024; Sourp et al., 2025) relative to LiDAR snow depth from Airborne Snow Observatory (ASO; Painter et al., 2016) surveys and gridded snow datasets (Broxton et al., 2024). Sourp et al. (2025) found that S1 retrievals exhibit no clear error pattern but consistently underestimate snow depth, particularly before and after the melt period**.** Broxton et al. (2024) found mean bias from 0.27m to 0.25m when compared against ASO LiDAR flights, depending on the removal of “flagged wet pixels”. Hoppinen et al. (2024) found that these flagged pixels do not fully eliminate wet pixels and remove some shallow dry snow pixels, resulting in a loss of usable data. Hoppinen et al. (2024) showed little to no spatial correlation between S1 and LiDAR data and with a mean root mean squared error (RMSE) of 0.92m, contrary to ~0.25m reported by Lievens et al. (2022). Evaluation studies

https://doi.org/10.5194/egusphere-2025-978
Preprint. Discussion started: 21 March 2025

(Broxton et al., 2024; Hoppinen et al., 2024) validate S1 data on a handful of dates near/after peak SWE with LiDAR surveys in the western U.S., while Lievens et al. (2022) conducted validation against point-scale time series at 1000s of locations in the European Alps and other global mountain ranges. Previous studies have shown that C-band S1 is ineffective near or after peak SWE due to the high liquid water content in the snowpack, which leads to the attenuation and absorption of microwave energy, (Gagliano et al., 2023; Nagler et al., 2016) leading to increased uncertainties in the retrieved snow depth. Thus, the spatial evaluation data (airborne LiDAR) are mostly available later in the snow season when S1 data are less reliable. Gascoin et al. (2024) highlights this limitation and recommends two strategies using S1 snow depth in a DA system: (1) assimilating S1 only during the early season when snow is dry, and (2) implementing a joint assimilation of S1 snow depth along with other remote sensing data (e.g., the snow disappearance date from optical snow-covered area data). To our knowledge, no studies have tested these strategies with S1 snow depth.

This paper aims to understand the spatiotemporal error discrepancies in S1 snow depth and assess how these data can be used in a DA system, both alone and in combination with other remote sensing data. First, we evaluate the S1 snow depth data (500 m resolution) using ground-based data at 12 sites and four airborne LiDAR flights in the well-studied East River Basin (Colorado, USA). Second, we develop a DA system using an ensemble-based model leveraging upon the recent development of the open-source toolbox Multiple Snow Data Assimilation System (MuSA) (Alonso-González et al., 2022) and deploy our DA system in a cloud-based environment. Using this system, we test whether assimilation of S1 snow depth across the full season (all observations) versus early season (when it is assumed to be most reliable) improves snow depth estimation in time and space, relative to snow simulations without assimilation. Finally, we test the joint assimilation of S1 snow depth and Moderate Resolution Imaging Spectroradiometer (MODIS) snow disappearance date (SDD) (Crumley et al., 2020) following the recommendation of Gascoin et al. (2024). We address three research questions:

https://doi.org/10.5194/egusphere-2025-978
Preprint. Discussion started: 21 March 2025

1. How do Sentinel-1 snow depth errors vary across space and time?
2. What is the relative value of using full-season Sentinel-1 data compared to early-season data in a data assimilation framework?
3. Can the joint assimilation of Sentinel-1 snow depth and MODIS snow disappearance date enhance DA accuracy?

2. Study Location and Data:

2.1. Study Location:

The study area is the East River Basin, Colorado (ERB Figure. 1a), which has ~300 km² area and features alpine tundra at higher elevations, montane forest at middle elevations, and prairie snow climates in lower elevation valleys (Sturm and Liston, 2021). It is characterized by cold winters, with a mean annual temperature of 0°C and mean annual precipitation of 1200m, mostly as snow (Daly et al., 1994; Hubbard et al., 2018). The ERB has an average elevation of 3266m with 1,420 m topographic relief. The ERB is ideal for this study because it has been well-studied and has extensive validation data through multiple scientific field campaigns, such as NASA SnowEx, ASO, the DOE SAIL (Feldman et al., 2023), and NOAA SPLASH. It also includes long-term NRCS SNOTEL sites within the basin (Butte) and nearby (e.g., Schofield Pass). In addition, ground measurements are available through a research site established in late 2018 on Snodgrass Mountain (Bonner et al., 2022), which was included in the 2020 NASA SnowEx campaign. Additionally, the ERB has been mapped by airborne LiDAR flight surveys carried out by ASO (Painter et al., 2016), which provided 50 m snow depth measurements twice in two study years (2018 and 2019). The study period spans water years 2018-2021, coinciding with the availability of S1 data and ASO data.

https://doi.org/10.5194/egusphere-2025-978
Preprint. Discussion started: 21 March 2025

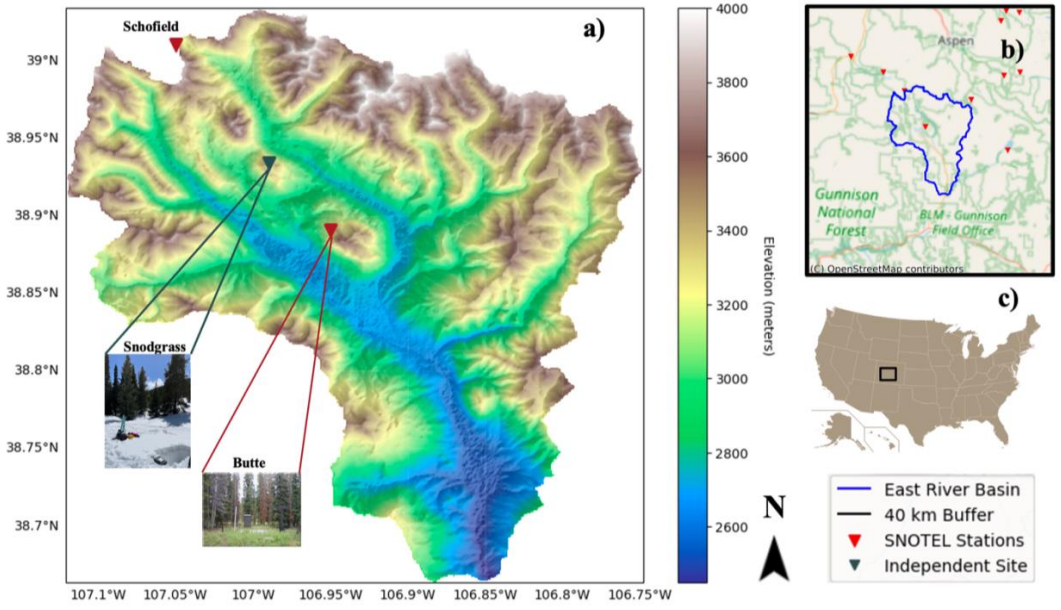

Figure 1: (a) Elevation map of the East River Basin(Jarvis et al., 2008) with Snodgrass and SNOTEL (USDA,NRCS, 2024) stations within and near the basin. **(b)** SNOTEL stations within 40km from the boundary of the basin. **(c)** Location of the East River Basin shown relative to the Western United States.

2.2. Data

2.2.1. Meteorological forcing:

ECMWF ERA5-Land reanalysis data (Hersbach et al., 2020) are used as the source of meteorological forcing data as they are available globally at a 0.1-degree (9 km) resolution hourly from 1981 to the present. The data, accessed from Google Cloud Storage, include incoming shortwave and longwave radiation [W m^{-2}], total precipitation (liquid and solid) [kg m^{-2} s^{-1}], surface atmospheric pressure [Pa], 2 m air temperature [K], 2 m relative humidity [%], and 10 m wind speed [m s^{-1}]. The data were not downscaled to the S1 500 m resolution because the DA approach implicitly accounts for fine-scale variability during assimilation (see below). In this implementation, a model ensemble is first generated at the original 9 km resolution and then regridded by nearest neighbor to 0.5 km resolution before applying the PBS, effectively capturing the downscaling process (Girotto et al., 2024; Smyth et al., 2019, 2020).

2.2.2. Sentinel-1 Snow Depth:

https://doi.org/10.5194/egusphere-2025-978
Preprint. Discussion started: 21 March 2025

We analyzed the 500 m S1 snow depth product (Lievens et al., 2022), which is available across mountainous regions of the Northern Hemisphere from 2016 to 2021. This dataset is derived from C-Band (5.4 GHz) SAR backscatter measurements collected by the ESA Sentinel-1A and Sentinel-1B satellites. The snow depth retrieval algorithm utilizes temporal variations in the ratio between cross-polarized and co-polarized backscatter signals, which are sensitive to snow depth in dry snow. Snow depth retrievals have reported mean absolute errors of 0.3m to 0.4m for snow depths between 0.5m to 2m (Lievens et al., 2022). However, the S1 performance degrades in challenging conditions (snow that is wet, shallow, patchy, or in forests) with a mean absolute error of about 1.3m at a depth of 3.5m and above (Lievens et al., 2022). Evaluation and development of this dataset is ongoing. The latest 500m dataset includes a quality flag for wet snow conditions, which has potential use for identifying and removing pixels with higher retrieval errors, particularly during the ablation season. Wet snow leads to the absorption and attenuation of radar signals, which makes snow depth mapping unreliable. The frequency of observations varies by region depending on the satellite overpass schedule. However, the dataset offers temporal resolution primarily on a daily to weekly basis, with most intervals being less than one week over the ERB.

2.2.3. Snow Disappearance Date (SDD):

We conduct multiple DA experiments (see Section 3.4), some of which utilize SDD as a baseline input in the assimilation to test whether S1 provides new information. We use SDD as a baseline because it is well established for guiding models in DA and SWE reconstructions. We derive SDD from different sources depending on the experiment. For the temporal evaluations, we derived SDD from SNOTEL by finding the first zero snow depth value after peak snow depth. For spatial evaluations, we derived SDD from MODIS snow cover data using annual summary metrics based on the daily Normalized Difference Snow Index (NDSI) from the MOD10A1 product with a threshold of 0.15, leveraging the SnowCloudMetrics algorithm implemented on Google Earth Engine (Crumley et al., 2020). The SDD is determined by identifying the last five snow-free days (backward approach) preceded by at least five consecutive snow-covered days. This approach minimizes the impact of transient late-season snow events while ensuring a consistent detection of snow disappearance.

2.2.4. Evaluation Data:

https://doi.org/10.5194/egusphere-2025-978
Preprint. Discussion started: 21 March 2025

We conduct temporal and spatial evaluations of snow depth, both prior to S1 assimilation and posterior to assimilation. Temporal evaluation utilizes daily snow depth from 11 NRCS SNOTEL stations within 40 km of the basin. Since the S1 change detection algorithm was optimized using SNOTEL data (Lievens et al., 2019), an independent research site at Snodgrass Mountain (Figure 1) was also utilized to assess the reliability of S1 snow depths away from SNOTEL sites. The Snodgrass Mountain site provides snow depth data, along with numerous monthly in situ snow pit measurements from February to May. These snow pits, located in both open and forested areas with a spatial extent of 1 km, are ideal for evaluating the 500 m S1 grid. S1 and posterior snow depths are evaluated against observations from these sites for WYs 2018–2021 for SNOTEL sites and 2019–2021 at the Snodgrass site.

The spatial evaluation uses four ASO LiDAR flights, with 50 m snow depth data collected near peak SWE (i.e., late March / early April) and in the mid-melt season (i.e., May or June) in 2018 and 2019 over the ERB. The data were resampled to match the 500 m S1 grid resolution using bilinear interpolation.

3. Methods:

3.1. DA Methodology

DA integrates model estimates with observations to estimate the most representative state of a system (e.g., SWE) with uncertainty. DA can account for observational uncertainty (e.g., S1 snow depth, MODIS SDD) and can provide physically consistent estimates of multiple snow states when implemented with a physically-based snow model. In this study, we develop and deploy a Python-based DA system in the Google Cloud Platform. Within the cloud, the system accesses ERA-5 Land meteorological data and uses it as input forcing into the MuSA toolbox, which communicates with the physically-based Flexible Snow Model version 2 (FSM2) model to generate ensembles of model simulations at a 9-km spatial resolution. The snow model ensembles from MuSA are combined with snow observations (e.g., S1 snow depth and/or SDD) via the particle batch smoother (PBS). Through assimilation of snow data with a wide ensemble (section 3.2), PBS also serves as a downscaling technique(Bachand et al., 2024) from the 9-km ERA5-Land forcings to the 500 m grid. The flow chart in Figure 2 and the sections below detail the key components.

https://doi.org/10.5194/egusphere-2025-978
Preprint. Discussion started: 21 March 2025

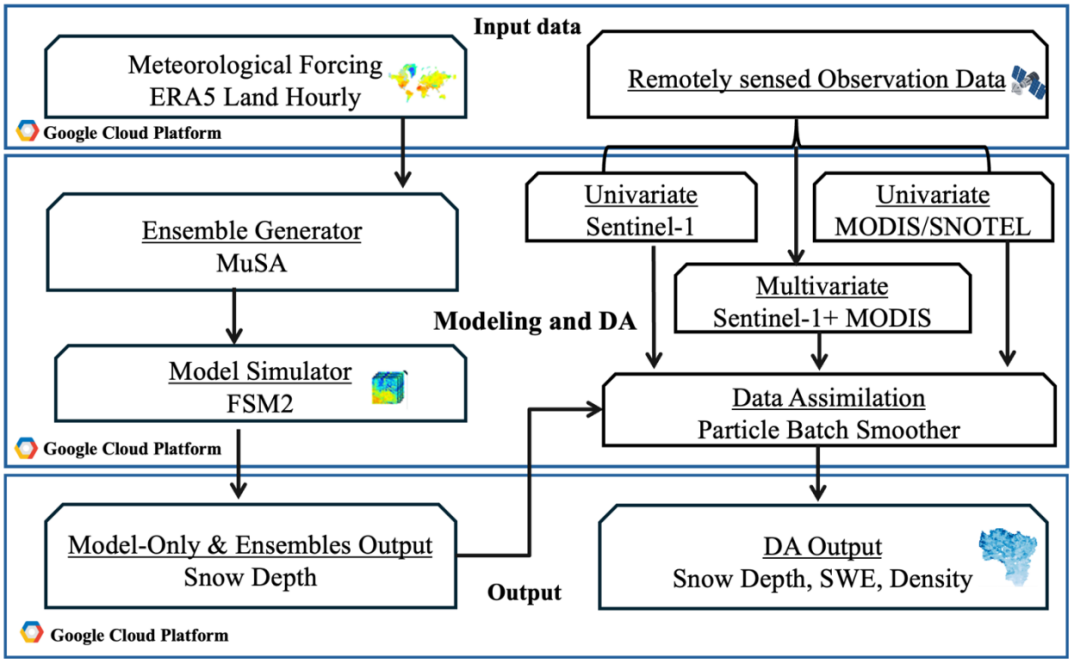

Figure 2. Flowchart illustrating the input, model and DA framework, and outputs (top to bottom).

3.2. Snow Model and Ensemble Generation:

FSM2 (Essery, 2015; Essery et al., 2024) is a multi-physics model that simulates the mass and energy balances of snow on the ground (including under forest canopies), employing three snow layers by default. The model incorporates conservation equations for liquid water, ice, and internal energy, offering a detailed representation of snowpack processes. FSM2's flexibility permits independent activation or deactivation of parameterizations, facilitating a range of model configurations (Essery, 2015; Essery et al., 2024). We utilize the most complex configuration of FSM2 to simulate internal snowpack processes, which we now briefly summarize. Albedo is calculated based on snow age, decreasing its value with time, and increasing it with fresh snowfalls. Snowpack thermal conductivity is determined by snow density, which is computed based on overburden and thermal metamorphism. Turbulent energy fluxes are computed based on bulk aerodynamic theory, and an adjustment for atmospheric stability is activated as part of the calculation process. Meltwater percolation in the snowpack is computed using gravitational drainage. The selected configuration has demonstrated success in related DA studies (Smyth et al., 2022).

https://doi.org/10.5194/egusphere-2025-978
Preprint. Discussion started: 21 March 2025

MuSA is an open-source, ensemble-based snow DA tool designed to assimilate multiple observations with FSM2 while considering various sources of forcing and measurement uncertainty (Alonso-González et al., 2022). We use MuSA to generate ensembles of FSM2 at a point scale. We perturbed the 9-km ERA5-Land hourly meteorological forcing data by drawing spatially independent, random perturbation parameters from a lognormal distribution for precipitation (to avoid negative values) and from a normal distribution for temperature and LW radiation (Table 1). Lower and upper bounds values for precipitation are selected to ensure realistic values, prevent negative values, and to account for downscaling. The standard deviation and mean values are used for temperature and LW radiation perturbations to represent variability and account for potential ERA5-Land biases. The perturbation strategy was chosen to ensure the ensemble spans a wide range of meteorological conditions and captures a realistic range of possible snow depths.

Table 1. Generation of perturbed inputs for each particle member.

Variable	Unit	Adjustment	Distribution	Lower Bound	Upper Bound	Std. dev.	Mean
Precipitation	mm/h	Multiplicative	Lognormal	0	4	-	-
Longwave radiation	W/m^2	Additive	Normal	-	-	20.8	0
Temperature	°C	Additive	Normal	-	-	2.5	0

Once the forcing data are perturbed, MuSA runs FSM2 to generate an ensemble of distinct snow simulations. We used 100 ensemble members (particles) to ensure computational efficiency while adequately capturing the variability in the prior distribution. For each particle, we record the SDD (i.e., the first snow-free date after peak snow depth), for use in multiple DA experiments (see Section 3.4).

3.3. Particle Batch Smoother – DA Algorithm

Once the ensembles are generated, we assimilate snow observations (e.g., snow depth and/or SDD) using the PBS algorithm. PBS employs a Bayesian approach, representing state variables like snow depth and SDD through a collection of particles, where each particle represents a possible system state. For observations within the assimilation window (e.g., snow season), PBS updates particle weights based on their likelihood of representing the true state, using the likelihood function from

https://doi.org/10.5194/egusphere-2025-978
Preprint. Discussion started: 21 March 2025

Margulis et al. (2015). This process combines the prior probability density function (PDF) with the likelihood to estimate the posterior PDF of snowpack variables, such as snow depth and SWE:

$$p_{Z|Y}(Z|Y) = p_V\left(Z - M_j^-\right) = \frac{1}{\sqrt{(2\pi)^{N_{obs}}|C_V|}} \times \exp\left[-0.5\left(Z - M_j^-\right)^\top C_V^{-1}\left(Z - M_j^-\right)\right] \quad \text{Equation (1)}$$

where **p(Z|Y)** is the likelihood function, which represents the probability of observing the measurement, **pV(V)** is the probability density function (PDF) of the measurement error vector V, **Z** is the observed measurement (e.g., S1 snow depth, MODIS SDD), $\mathbf{M_j}$ is the modeled snow variable (e.g., snow depth or SDD), and $\mathbf{C_v}$ is the error covariance matrix of the measurement error vector V, which represents the uncertainty in the measurement.

3.4. DA Experiments

To address Research Questions 2 and 3, we conducted four experiments, building on the findings of Research Question 1 (S1 error analysis). The DA experiments are as follows (Figure 3):

1. Snow Depth (**Hs**) **F**ull Window **(Hs-F):** Assimilation of all Hs, including dry and wet snow pixels, from November 15th to April 30th. S1 has data only until April 30th, and 83% of S1 data points before November 15th have zero or less than 10cm snow depth values. Thus, we call Hs-F a full-window experiment.

2. Snow Depth (**Hs**) **E**arly Window **(Hs-E):** Assimilation of early-season (November 15th to January 15th) Hs, where the early window has a lower observational error than the full window (based on error analysis, section 4.1).

3. Joint Assimilation of SDD and Snow Depth in the **F**ull Window **(SDD+Hs-F):** Combined assimilation of SDD and Hs over the same window as Hs-F. SDD data were derived from SNOTEL for temporal evaluation and MODIS for spatial evaluation.

4. **S**now **D**isappearance **D**ate Only **(SDD):** Assimilation of SDD data alone, derived from SNOTEL (temporal evaluations) or MODIS (spatial evaluations). This serves as a baseline or control experiment to understand whether S1 snow depth adds new information.

https://doi.org/10.5194/egusphere-2025-978
Preprint. Discussion started: 21 March 2025

SDD is the baseline experiment and each of it is evaluated against 12 ground-based stations temporally and 4 ASO LiDAR flights spatially (Section 2.2.2). In experiments Hs-F, Hs-E, and SDD+Hs-F, the observational uncertainty value (Equation 1) for S1 snow depth is the RMSE when evaluated against SNOTEL for all four years. The SDD observational uncertainty is set to five days, consistent with the retrieval algorithm in SnowCloudMetrics (Crumley et al., 2020). In the joint assimilation (SDD+Hs-F), both datasets are weighted equally to balance their respective influence in DA:

$$\mathbf{p(Z \mid Y)} = \mathbf{p(Z\_Hs \mid Y)} + \mathbf{p(Z\_SDD \mid Y)} \quad \text{Equation (2)}$$

where **p(Z_Hs|Y)** is the snow depth and **p(Z_SDD|Y)** is the SDD likelihood function. This equal-weight approach for joint assimilation is necessary for two reasons: (1) there is an imbalance in the number of observations for Hs (dozens of observations) versus SDD (1 value) for each location and year, and (2) the Hs time series exhibits temporal autocorrelation.

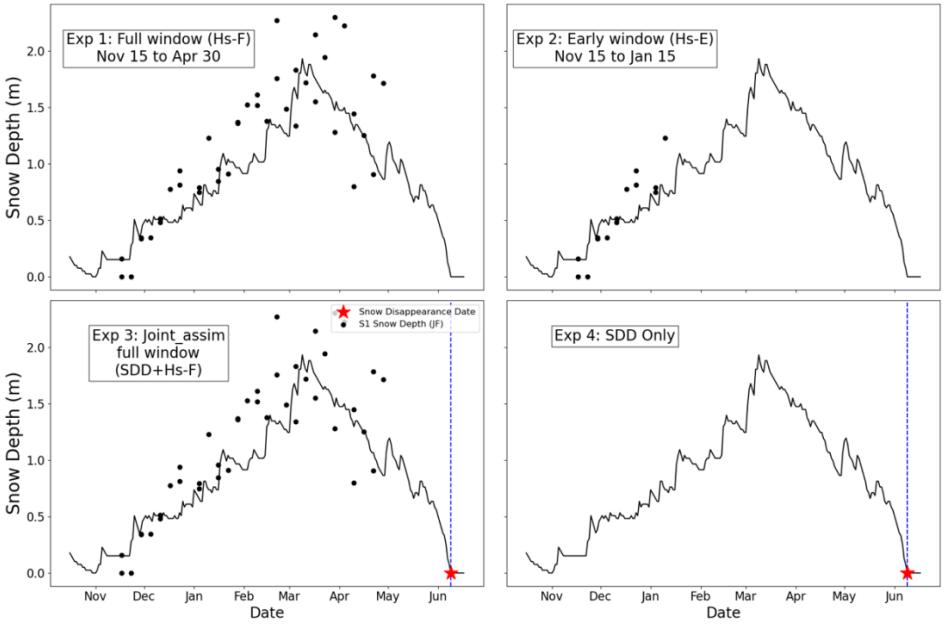

Figure 3. Conceptual illustration of four experiments. Black dots indicate S1 observation data, black lines represent posterior estimates, and red stars (with blue dashed line) denote the SDD.

3.5. Evaluation

https://doi.org/10.5194/egusphere-2025-978
Preprint. Discussion started: 21 March 2025

We evaluated snow depth (i.e., S1 observations and PBS experiments) with standard valuation metrics, including coefficient of determination (R^2), root mean squared error (RMSE), mean bias, mean absolute error (MAE), and relative mean absolute difference (RMAD). These were selected to enable comparisons to other studies (Lievens et al., 2019; Broxton et al., 2024; Hoppinen et al., 2024). MAE and RMAD are defined as:

$$MAE = \frac{1}{n}\sum|y_i - \hat{y}_i| \qquad \text{Equation (3)}$$

$$RMAD = \frac{\frac{1}{n}\sum_i|\hat{y}_i - y_i|}{\overline{y}} \qquad \text{Equation (4)}$$

where y_i is the observed value (e.g., LiDAR, SNOTEL, field data), $\hat{y}_i$ is the predicted value (e.g., PBS posterior mean), $\overline{y}$ is the mean of all observed/validation data values, and n represents the total number of data points.

4. Results

4.1 Error Analysis

Errors in the S1 500m snow depth data were evaluated temporally at 11 SNOTEL stations and an independent site (Snodgrass) from 2018–2021 and spatially relative to ASO LiDAR flights in 2018 and 2019. We included wet/flagged pixels in all our analyses/experiments because the removal of flagged pixels resulted in performance degradation (results not shown). The results are shown in Table 2.

Table 2. Average R^2, RMSE, Mean Bias, MAE, and RMAD values of **(a)** S1 against an 11 SNOTEL sites and the Snodgrass site. (b) S1 against ASO 50m LiDAR snow depth aggregated to 500m.

	(a) Temporal evaluation – average across all stations **(m)**					**(b)** Spatial evaluation – **S1 against ASO LiDAR (m)**		
Year	**2018**	**2019**	**2020**	**2021**	**Average**	**2018**	**2019**	**Average**
R^2	0.74	0.80	0.72	0.72	0.74	0.19	0.27	0.23
RMSE	0.32	0.39	0.39	0.53	0.40	0.74	0.91	0.82
Mean Bias	0.08	-0.07	0.09	0.26	0.09	-0.47	-0.26	-0.36
MAE	0.21	0.26	0.27	0.38	0.28	0.60	0.72	0.66
RMAD	0.61	0.39	0.47	0.68	0.53	0.77	0.43	0.60

https://doi.org/10.5194/egusphere-2025-978
Preprint. Discussion started: 21 March 2025

S1 had bias of +0.09 m, RMSE of 0.40 m and R^2 of 0.74 when evaluated temporally against stations. In contrast, when evaluated spatially against ASO, S1 had higher bias (-0.36 m), higher RMSE (0.82 m), and lower R^2 (0.23) (Table 2). These results indicated that S1 performed better in capturing temporal variations compared to spatial patterns. S1 errors tended to increase over time across all stations (Figure 4), with the lowest errors in the early season and the highest errors near peak snow depth. The timing of the two LiDAR flights coincided with the time of year when errors tend to be high (thick grey vertical lines, Fig. 4).

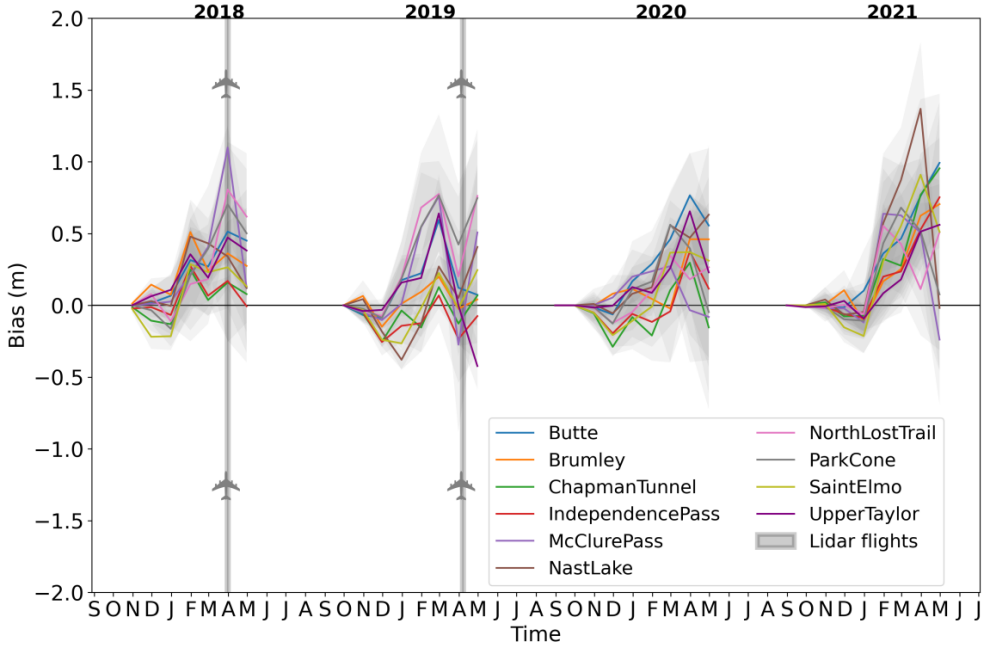

Figure 4: Time-varying errors at the 11 SNOTEL sites with LiDAR flight marked with thick grey lines. The solid lines represent the monthly mean bias, while the shaded region represents the range of error. Each station is represented by a different color.

4.2. Temporal Window Experiments:

Next, we assessed the performance of S1 assimilation with respect to window size, i.e., full window data assimilation (Hs-F) compared to the early window (Hs-E) when errors were lower (Fig. 4). The results are shown in Figure 5 for two sites: (1) an independent site (Snodgrass), which was not used in the optimization of the S1 dataset, and (2) a representative SNOTEL site. The time series of the two sites shows that the performance of Hs-F and Hs-E is not consistent across the years. Hs-F (black line) performed marginally better than Hs-E (green line) in WY 2019 and similarly in

https://doi.org/10.5194/egusphere-2025-978
Preprint. Discussion started: 21 March 2025

2020 and 2021 for the Snodgrass site. Likewise, Hs-F performed better than Hs-E in WY 2018, poorly in 2021, and similarly in 2019 and 2020 at Chapman Tunnel.

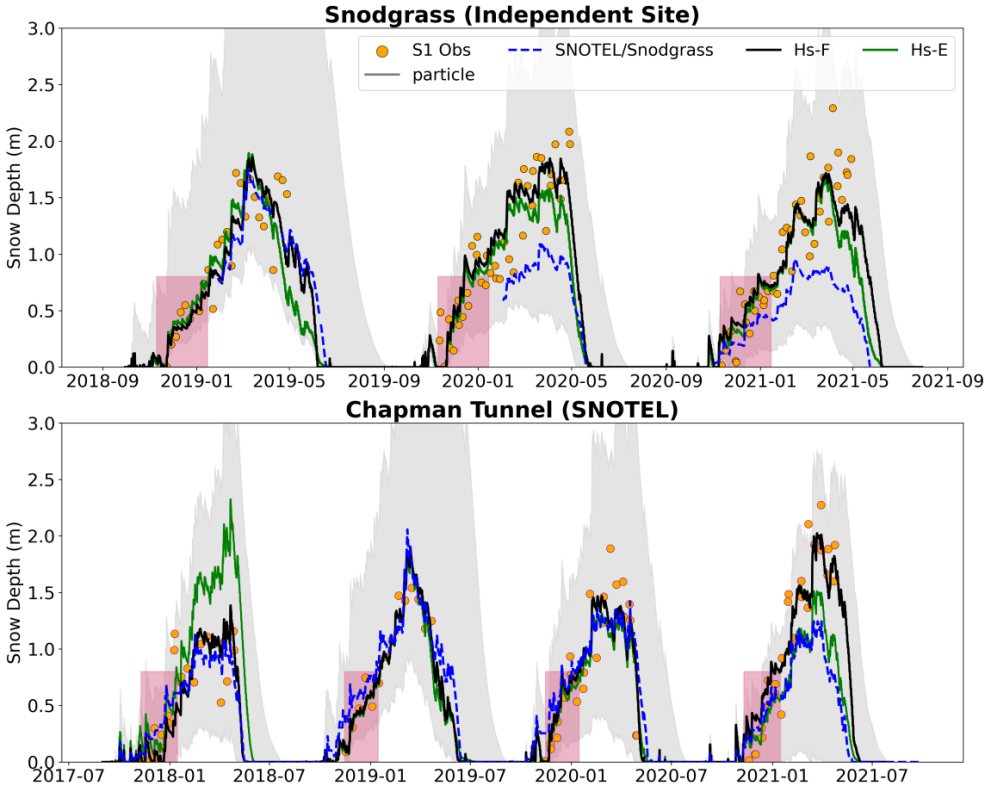

Figure 5: Temporal analysis results at (top) Snodgrass and (bottom) Chapman Tunnel. Hs-F (black line) and Hs-E (green line) represent the posterior mean of full and early window experiments. SNOTEL and Snodgrass station data (blue dashed line) provide snow depth evaluation data. Purple dots represent S1 snow depth observations. Gray shading indicates one standard deviation of particle spread and the pink rectangle highlight the early assimilation window.

The statistical analysis across temporal evaluation sites give insights into the average performance of each DA window experiment. The results show RMSE of 0.29 m for Hs-F and 0.35 m for Hs-E, while R^2 is 0.87 for Hs-F and 0.84 for Hs-E (Table 3). Overall, the differences between Hs-F and Hs-E across all sites and evaluation metrics are minimal, suggesting that the accuracy of S1 snow depth retrievals remains consistent regardless of the temporal window. This implies that the retrieval method performs similarly for both the full and early windows.

https://doi.org/10.5194/egusphere-2025-978
Preprint. Discussion started: 21 March 2025

Table 3: Error metrics of posterior mean of Hs-F (full window assimilation) and Hs-E (early window assimilation). Metrics are averaged across all temporal evaluation sites and across four years.

Metrics	Experiments	
	Hs-F	Hs-E
R^2	0.88	0.86
RMSE (m)	0.29	0.35
Mean Bias (m)	0.07	0.09
MAE	0.20	0.23
RMAD	0.46	0.63

While the temporal analysis shows a marginal difference in Hs-F and Hs-E, spatial analysis reveals a significant disparity in performance, with Hs-F outperforming Hs-E significantly across all LiDAR flights consistently in most metrics (Table 4). For example, Hs-F demonstrates a lower average RMSE (0.66 m vs. 0.91 m), lower mean bias (0.05m vs. -0.61m) along with lower MAE (0.42m vs. 0.75m) and RMAD (0.61 vs. 1.2m) compared to Hs-E. However, Hs-F performs slightly worse in specific survey dates, such as R^2 on 2019-06-10, where Hs-E performs better than Hs-F (0.08 vs. 0.57m). The temporal and spatial RMSE across all stations and years and LiDAR flights are shown in Figure 6, showing lower RMSE in all cases except in the 2019-06-10 LiDAR flight. The density plots (Figure 7c) compare the posterior mean snow depths from the full-window (Hs-F) and early-window (Hs-E) assimilation experiments with LiDAR measurements. The density distribution aligns with LiDAR only in certain cases (Fig. 7c), reflecting both experiments perform consistently poor relative to the LiDAR snow depths. Across all four LiDAR surveys, the spatial patterns in snow depth are not strongly related (i.e., R^2<0.60) for either Hs-E or Hs-F (Table 4, Figure 7). The overall analysis indicates that S1 has high errors spatially regardless of window, but the full-window assimilation approach (Hs-F) provides relatively lower errors across spatial locations and LiDAR dates (Figure 7). Therefore, Hs-F is utilized as the optimal window for the rest of the data assimilation experiments (see Section 4.3).

https://doi.org/10.5194/egusphere-2025-978
Preprint. Discussion started: 21 March 2025

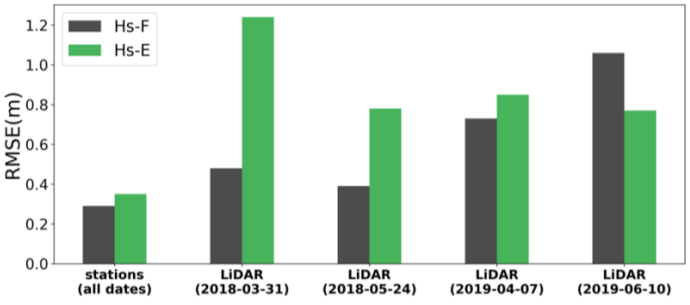

Figure 6. Bar chart comparing average RMSE from the Hs-F and Hs-E experiments when evaluated at the 12 snow stations. The average errors are shown for all dates and on each of the four LiDAR flight dates.

Table 4. Error metrics for the posterior mean snow depth from the Hs-F, Hs-E, and control experiments when evaluated against snow depth from four LiDAR surveys.

LiDAR Survey	Exp	R^2	RMSE (m)	Mean Bias (m)	MAE (m)	RMAD (m)
2018-03-31	Hs-F	0.51	0.48	-0.21	0.35	0.45
	Hs-E	0.29	1.24	-1.15	1.15	1.48
2018-05-24	Hs-F	0.33	0.39	0.08	0.21	0.88
	Hs-E	0.37	0.78	-0.59	0.69	2.55
2019-04-07	Hs-F	0.33	0.73	-0.08	0.52	0.31
	Hs-E	0.47	0.85	-0.52	0.66	0.40
2019-06-10	Hs-F	0.08	1.06	0.44	0.60	0.83
	Hs-E	0.57	0.77	-0.21	0.52	0.63
Average	**Hs-F**	**0.31**	**0.66**	**0.05**	**0.42**	**0.61**
	Hs-E	**0.42**	**0.91**	**-0.61**	**0.75**	**1.2**

https://doi.org/10.5194/egusphere-2025-978
Preprint. Discussion started: 21 March 2025

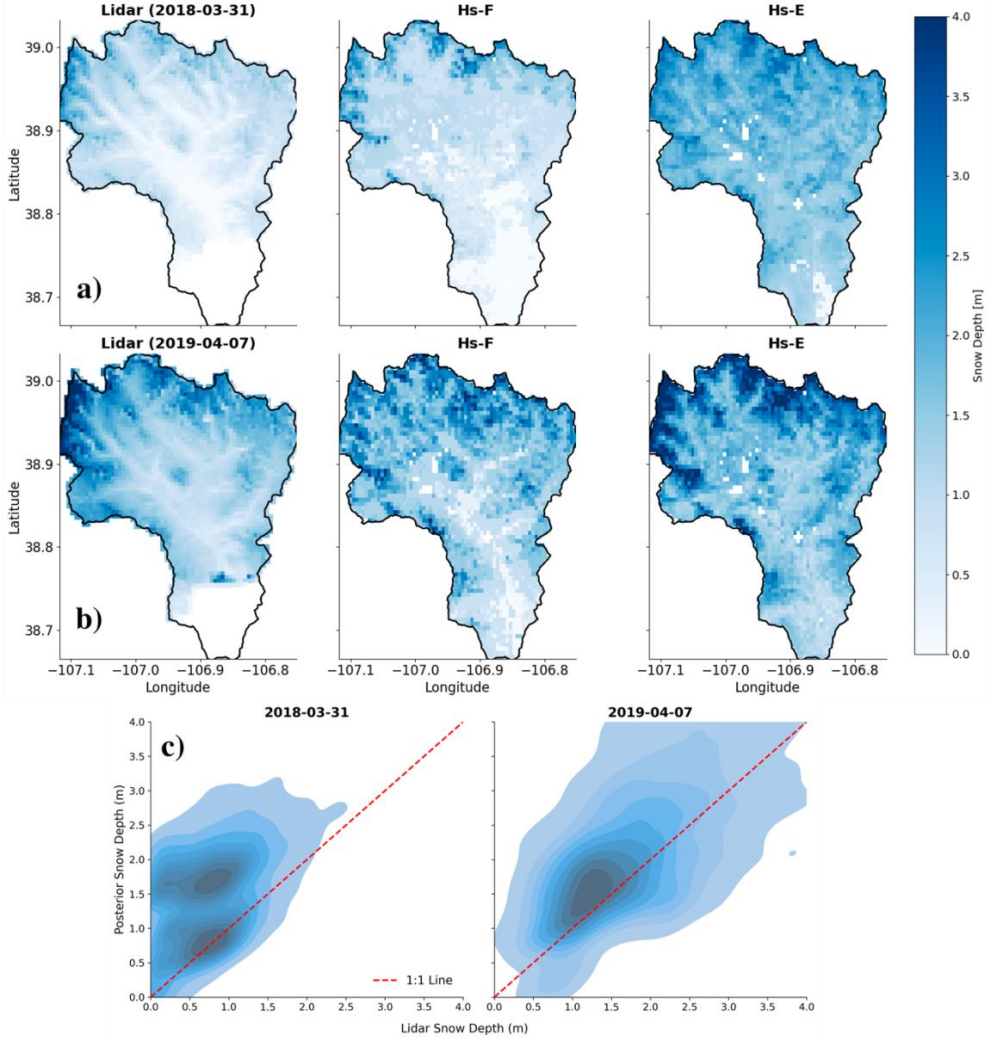

Figure 7: The first column in panels a and b shows snow depth from airborne LiDAR near peak snow accumulation. The second and third columns in panels a and b show the posterior mean snow depth from the Hs-F and Hs-E experiments, respectively. Panel c shows the density plot comparing two experiments (Hs-F and Hs-E) against LiDAR measurements. Since both experiments showed similar correlations with LiDAR, they are combined into a single plot.

4.3. Joint Assimilation Experiments:

Finally, we evaluate the joint assimilation of SDD+Hs-F against SDD alone (baseline) to test the utility of S1 snow depth for adding new information to a DA system. We utilized Hs-F than Hs-E

https://doi.org/10.5194/egusphere-2025-978
Preprint. Discussion started: 21 March 2025

because errors tended to be lower with Hs-F (see section 4.2). The temporal results of experiments 3 and 4 of the most representative and independent site are shown in Figure 8. The temporal results show that the performance of Hs-F (experiment 1), SDD+Hs-F (experiment 3), and SDD alone (experiment 4) varies across the years. Hs-F performed better than SDD-Hs-F and SDD in WY 2019 and 2020 and consistently in 2021 for the Snodgrass site. In the SNOTEL representative site, SDD performed better or consistently with Hs-F and SDD+Hs-F in all WYs. The statistical temporal analysis indicates that joint assimilation and SDD alone experiments perform better than Hs-F minimally across all metrics (~0.01m). However, the performance of SDD+Hs-F is approximately the same as the baseline SDD experiment (Table 5), suggesting that joint assimilation of SDD with S1 snow depth does not significantly enhance performance relative to just assimilating SDD alone.

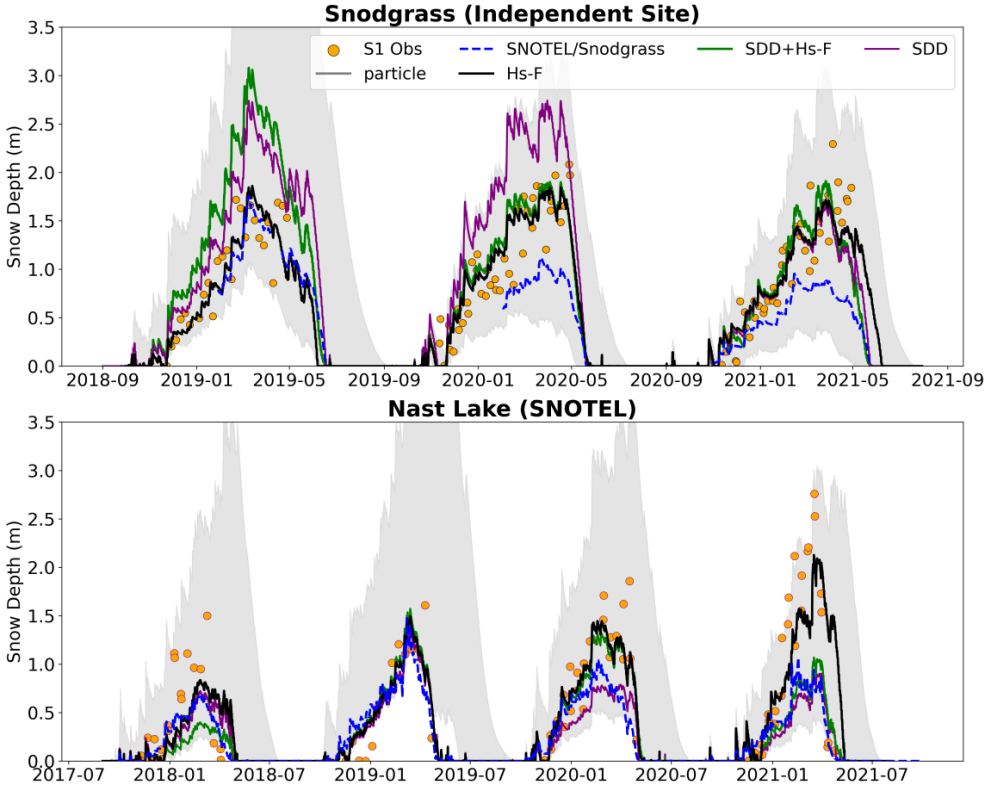

Figure 8: Example results of the joint assimilation experiments at (a) Snodgrass and (b) Nast Lake. Hs-F (black line) and SDD+Hs-F (green line) represent the posterior mean for each experiment. SDD (purple line) is the posterior snow depth based on assimilating only SDD. SNOTEL and Snodgrass in situ (blue

https://doi.org/10.5194/egusphere-2025-978
Preprint. Discussion started: 21 March 2025

dashed line) provide snow depth evaluation data. Orange dots represent S1 snow depth observations. Gray shading indicates one standard deviation of particles.

Table 5. Error metrics of posterior mean of Hs-F (full window assimilation), SDD+HS-F (joint assimilation), and SDD. Metrics are averaged across all temporal evaluation sites and across four years.

Metrics	Experiments	
	SDD+Hs-F	SDD
R^2	0.92	0.92
RMSE	0.28	0.28
Mean Bias	0.15	0.14
MAE	0.19	0.19
RMAD	0.42	0.43

Spatial analysis provides more insights on the evaluation of SDD assimilations, both in univariate (Hs-F or SDD) and joint assimilation experiments (Hs-F+SDD). Across all metrics, assimilating SDD alone results in higher performance compared to both Hs-F and SDD+Hs-F. The temporal and spatial RMSE across all stations, years, and LiDAR flights is shown in Figure 9. The RMSE is 0.41 m for SDD assimilation averaged across all LiDAR flights and years, which is lower than the RMSE of Hs-F (0.66 m, Table 4) and SDD+Hs-F (0.70 m, Table 6). Additionally, assimilating SDD alone demonstrates a stronger relationship with LiDAR observations (R^2 = 0.72) compared to Hs-F (R^2 = 0.31) and SDD+Hs-F (R^2 = 0.46), with better spatial pattern alignment across both LiDAR dates near peak accumulation (Table 6, Fig. 10). Joint assimilation (SDD+Hs-F) shows lower performance in comparison to Hs-F alone or SDD alone, suggesting that the combination of S1 with SDD does not enhance performance and may potentially degrade it.

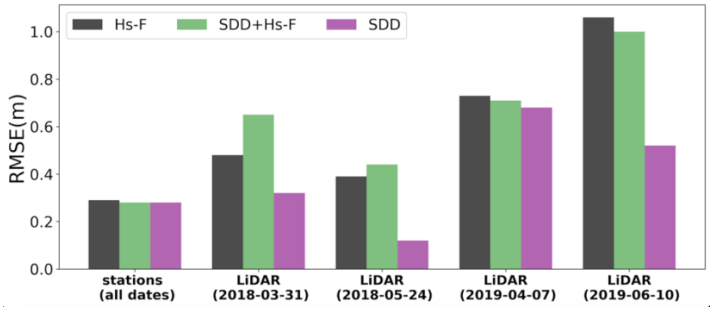

Figure 9: Bar chart comparing RMSE for Hs-F, SDD+Hs-F, and SDD experiments of stations (SNOTEL+Snodgrass) averaged across all stations and all four years, and each LiDAR flight.

https://doi.org/10.5194/egusphere-2025-978
Preprint. Discussion started: 21 March 2025

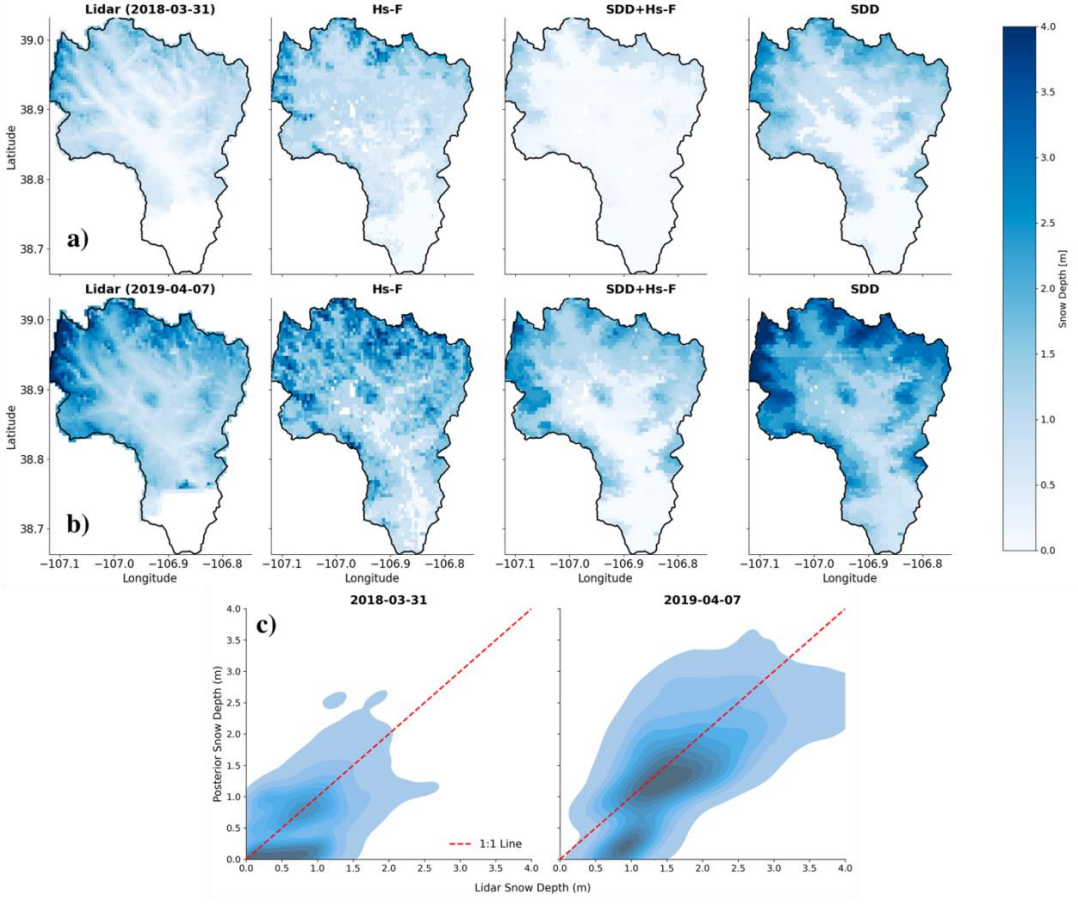

Figure 10: The first column in panels a and b shows snow depth from airborne LiDAR near peak snow accumulation. The second, third, and fourth columns in panels a and b show the posterior mean snow depth from the Hs-F, SDD+Hs-F, and SDD experiments, respectively. Panel c shows the density plot comparing two experiments (Hs-F, SDD-Hs-F, and SDD) against LiDAR measurements. Since both experiments showed similar correlations (or better in the case of SDD) with LiDAR, they are combined into a single plot.

Table 6. Error metrics of posterior mean snow depth from the SDD+Hs-F and SDD experiments when evaluated against four LiDAR surveys.

LiDAR Survey	Exp	R^2	RMSE (m)	Mean Bias (m)	MAE (m)	RMAD (m)
2018-03-31	SDD+Hs-F	0.58	0.65	0.55	0.55	0.71
	SDD	0.74	0.32	-0.25	0.33	0.42

https://doi.org/10.5194/egusphere-2025-978
Preprint. Discussion started: 21 March 2025

2018-04-24	SDD+Hs-F	0.10	0.44	0.23	0.23	0.99
	SDD	0.70	0.12	-0.01	0.13	0.53
2019-04-07	SDD+Hs-F	0.69	0.71	0.55	0.62	0.35
	SDD	0.70	0.68	-0.48	0.54	0.32
2019-06-10	SDD+Hs-F	0.49	1.0	0.71	0.71	0.85
	SDD	0.76	0.52	-0.09	0.34	0.40
Average	**SDD+Hs-F**	**0.46**	**0.70**	**0.51**	**0.52**	**0.72**
	SDD	**0.72**	**0.41**	**0.20**	**0.33**	**0.42**

5. Discussion:

This study evaluates the utility of S1 SAR-derived snow depth data in the mountainous ERB (Colorado) to support spatiotemporal snow depth mapping within a DA framework. Our analysis highlights inconsistencies in temporal versus spatial errors in S1 snow depth data. While S1 demonstrates lower temporal errors (RMSE = 0.40 m, R^2 = 0.74), spatial errors were higher (RMSE = 0.82m, R^2 = 0.23) relative to LiDAR flights near or after peak accumulation. Temporal errors were lower during the early season but increased over time, particularly during the ablation phase when wet snow conditions become more likely. These discrepancies align with prior studies (Broxton et al., 2024; Hoppinen et al., 2024), which report significant errors in S1 snow depth data under wet snow conditions and poor spatial correlations with airborne LiDAR data (RMSE > 0.7 m, R^2 < 0.3). The limitation may also stem from the timing of validation data, as most LiDAR flights are conducted near or after peak snow depth when S1 performance is most likely compromised due to wet snow. Unlike prior studies that proposed excluding flagged wet pixels as a mitigation strategy, we found that removing flagged pixels increased errors, potentially due to the omission of shallow dry snow observations (Hoppinen et al., 2024). Lievens et al. (2022) reported significantly lower errors (~0.25 m) in the European Alps, which is contrary to studies (Broxton et al., 2024; Hoppinen et al., 2024) focused on the Western US, including our study. The lower error reported by Lievens et al. (2022) could be due to a higher overpass frequency and denser validation datasets and needs further investigation.

Our DA experiments were informed by the recommendations of Gascoin et al. (2024) and aimed to determine the optimal assimilation window (full season vs. early season) for generating spatiotemporal snow depth maps using multiple remote sensing observations (i.e., S1 snow depth

https://doi.org/10.5194/egusphere-2025-978
Preprint. Discussion started: 21 March 2025

and MODIS SDD). The comparison between the full-window (Hs-F) and early-window (Hs-E) approaches showed minimal improvement in error metrics in the temporal analysis at ground-based stations. Spatial evaluations against LiDAR data resulted in Hs-F performing better than Hs-E. However, Hs-F increases the likelihood of including wet snow conditions and higher errors later in the snow season, suggesting a trade-off between data volume and data quality (Figure. 4). The early-window approach benefits from reduced retrieval errors due to its focus on lower snow depth values and assumed higher likelihood of dry snow in December and January. However, this approach is more effective in regions where a significant fraction of the total SWE accumulates early in the season (Lundquist et al., 2023). In contrast, basins like the ERB receive significant snowfall after January, which reduces the early-season window's ability to predict SWE reliably later in the year (e.g., April-onward). This seasonal snow accumulation pattern likely explains why the early-window approach is less effective in our study. This variability underscores the inherent challenges in using early-season conditions to make broader inferences about snowpack dynamics later in the year. Despite these limitations, the results show that errors in S1 snow depth retrievals are relatively independent of the assimilation window.

The joint assimilation of S1 snow depth with SDD was conducted to understand what information is added by S1 and to test whether SDD can provide additional constraints on the DA outcome. Previous studies successfully used joint assimilation in a DA system with satellite data such as ICESat-2 (Mazzolini et al., 2024). However, joint assimilation showed limited value with S1 snow depth data: The errors did not decrease when assimilating S1 depth with SDD. Assimilating SDD alone showed a higher R^2 value and lower errors on average compared to Hs-F and SDD+Hs-F.

There are some caveats and potential limitations in the study. This study focused on a single basin and a limited number of nearby snow pillow stations over a four-year period. A more comprehensive evaluation against LiDAR data has already been conducted with the available LiDAR data in the western U.S. (Broxton et al., 2024; Hoppinen et al., 2024. Similar to previous studies, we were also limited by the evaluation LiDAR data since it was only available at peak snow depth or in the melt season, when S1 has higher errors. This highlights the importance of expanding spatial and temporal coverage of evaluation data.

https://doi.org/10.5194/egusphere-2025-978
Preprint. Discussion started: 21 March 2025

Future research should continue to develop and explore approaches for using Sentinel-1 and other spaceborne remote sensing platforms for mapping SWE and other related snowpack variables. One established capability of S1 backscatter data is for wet snow mapping (Gagliano et al., 2023; Nagler et al., 2016). For snow depth and SWE mapping, the existing Lievens et al. (2019) algorithm may be improved through corrections with machine learning as proposed by Broxton et al. (2024). Alternatively, interferometric SAR (InSAR) techniques (Oveisgharan et al., 2024) have recently been shown to have some potential for mapping SWE with S1 C-band data, although challenges related to the frequency of satellite passes remain a challenge (Deeb et al., 2011) and these techniques are likely more reliable with L-band SAR data. The upcoming NISAR mission will provide L-band SAR data, which may provide new opportunities for accurate snow depth mapping in mountainous regions that may overcome the current limitations of C-band SAR.

6. Conclusion

This study underscores the challenges of using C-Band S1 SAR-derived snow depth data within a DA framework. While S1 is currently the only high-resolution (<1 km) remotely sensed snow depth dataset available across the Northern Hemisphere, it demonstrated notable biases and limitations in snow depth mapping, particularly near and after maximum snowpack accumulation which has high hydrologic significance. These errors were similar across both full-window and early-window assimilation experiments and align with prior studies that reported significant spatial biases and retrieval errors, particularly under wet snow conditions. The joint assimilation of S1 snow depth with SDD data showed limited or no improvement, suggesting that assimilating SDD alone yields greater accuracy.

While recognizing that our study focused on a single mountain basin, we conclude that the reliability of the current S1 snow depth retrieval algorithm presents major challenges for a snow DA system. Future research should prioritize algorithm improvements, explore machine learning techniques, and conduct additional testing across a wider range of basins and with spatial data. Enhanced methods for snow depth monitoring would improve understanding of snowpack dynamics in regions where ground-based observations are sparse or unavailable, supporting better water resource management and climate impact assessments.

https://doi.org/10.5194/egusphere-2025-978
Preprint. Discussion started: 21 March 2025

Author Contributions: Data curation and Analysis: BM. Experiment Design: BM, MR, EE. Writing: The draft was led by BM with key contribution and editing by all co-authors. Funding Acquisition: MR and ES.

Code and data availability: This study used airborne LiDAR snow depth data (ASO, Inc.), MODIS and ERA5 data (GEE), NRCS SNOTEL, and independent validation data from teams at the University of Colorado and Oregon State University. The MuSA code, which integrates FSM, is available at https://github.com/ealonsogzl/MuSA, with FSM originally developed by Richard Essery. Computational resources were provided by Oregon State University's College of Engineering.

Competing interests: The authors declare that they have no conflict of interest.

Acknowledgments

This work was supported by the National Aeronautics and Space Administration (NASA) Terrestrial Hydrology Program under Award No. 80NSSC22K0685. The authors thank Esteban Alonso González for making the MuSA code available (https://github.com/ealonsogzl/MuSA) and Richard Essery for development of FSM. This work utilized resources from Oregon State University College of Engineering high-performance computing network. The independent temporal validation data was collected by student teams from the University of Colorado (Eric Small Hydrology Group) and Oregon State University (CryoSphere Interactions and Geospatial Hydrology Team). The authors also thank the ASO, Inc. team for providing the airborne LiDAR snow depth and GEE for facilitating the access of MODIS and meteorological forcing data used in the study.

https://doi.org/10.5194/egusphere-2025-978
Preprint. Discussion started: 21 March 2025

References:

Aalstad, K., Westermann, S., and Bertino, L.: Evaluating satellite retrieved fractional snow-covered area at a high-Arctic site using terrestrial photography, Remote Sensing of Environment, 239, 111618, https://doi.org/10.1016/j.rse.2019.111618, 2020.

Alonso-González, E., Aalstad, K., Baba, M. W., Revuelto, J., López-Moreno, J. I., Fiddes, J., Essery, R., and Gascoin, S.: The Multiple Snow Data Assimilation System (MuSA v1.0), Geosci. Model Dev., 15, 9127–9155, https://doi.org/10.5194/gmd-15-9127-2022, 2022.

Bachand, C., Andrews, L. C., Rouf, T., and Girotto, M.: The Utility of Satellite Snow Depth Observations for Downscaling Hydrologic Variables Over the Indus Basin Mountain Ranges, https://doi.org/10.2139/ssrn.4880050, 2024.

Barnett, T. P., Adam, J. C., and Lettenmaier, D. P.: Potential impacts of a warming climate on water availability in snow-dominated regions, Nature, 438, 303–309, https://doi.org/10.1038/nature04141, 2005.

Besso, H., Shean, D., and Lundquist, J. D.: Mountain snow depth retrievals from customized processing of ICESat-2 satellite laser altimetry, Remote Sensing of Environment, 300, 113843, https://doi.org/10.1016/j.rse.2023.113843, 2024.

Bonner, H. M., Smyth, E., Raleigh, M. S., and Small, E. E.: A Meteorology and Snow Data Set From Adjacent Forested and Meadow Sites at Crested Butte, CO, USA, Water Resources Research, 58, https://doi.org/10.1029/2022WR033006, 2022.

Brangers, I., Lievens, H., Getirana, A., and De Lannoy, G. J. M.: Sentinel-1 Snow Depth Assimilation to Improve River Discharge Estimates in the Western European Alps, Water Resources Research, 60, e2023WR035019, https://doi.org/10.1029/2023WR035019, 2024.

Broxton, P., Ehsani, M. R., and Behrangi, A.: Improving Mountain Snowpack Estimation Using Machine Learning With Sentinel-1, the Airborne Snow Observatory, and University of Arizona Snowpack Data, Earth and Space Science, 11, e2023EA002964, https://doi.org/10.1029/2023EA002964, 2024.

Broxton, P. D., Van Leeuwen, W. J. D., and Biederman, J. A.: Improving Snow Water Equivalent Maps With Machine Learning of Snow Survey and Lidar Measurements, Water Resources Research, 55, 3739–3757, https://doi.org/10.1029/2018WR024146, 2019.

Chang, A. T. C., Foster, J. L., and Hall, D. K.: Nimbus-7 SMMR Derived Global Snow Cover Parameters, A. Glaciology., 9, 39–44, https://doi.org/10.3189/S0260305500200736, 1987.

Clark, M. P., Hendrikx, J., Slater, A. G., Kavetski, D., Anderson, B., Cullen, N. J., Kerr, T., Örn Hreinsson, E., and Woods, R. A.: Representing spatial variability of snow water equivalent in hydrologic and land-surface models: A review, Water Resources Research, 47, 2011WR010745, https://doi.org/10.1029/2011WR010745, 2011.

https://doi.org/10.5194/egusphere-2025-978
Preprint. Discussion started: 21 March 2025

Cluzet, B., Lafaysse, M., Deschamps-Berger, C., Vernay, M., and Dumont, M.: Propagating information from snow observations with CrocO ensemble data assimilation system: a 10-years case study over a snow depth observation network, The Cryosphere, 16, 1281–1298, https://doi.org/10.5194/tc-16-1281-2022, 2022.

Crumley, R. L., Palomaki, R. T., Nolin, A. W., Sproles, E. A., and Mar, E. J.: SnowCloudMetrics: Snow Information for Everyone, Remote Sensing, 12, 3341, https://doi.org/10.3390/rs12203341, 2020.

Daly, C., Neilson, R. P., and Phillips, D. L.: A Statistical-Topographic Model for Mapping Climatological Precipitation over Mountainous Terrain, J. Appl. Meteor., 33, 140–158, https://doi.org/10.1175/1520-0450(1994)033<0140:ASTMFM>2.0.CO;2, 1994.

Deeb, E. J., Forster, R. R., and Kane, D. L.: Monitoring snowpack evolution using interferometric synthetic aperture radar on the North Slope of Alaska, USA, International Journal of Remote Sensing, 32, 3985–4003, https://doi.org/10.1080/01431161003801351, 2011.

Derksen, C., Walker, A., and Goodison, B.: Evaluation of passive microwave snow water equivalent retrievals across the boreal forest/tundra transition of western Canada, Remote Sensing of Environment, 96, 315–327, https://doi.org/10.1016/j.rse.2005.02.014, 2005.

Deschamps-Berger, C., Cluzet, B., Dumont, M., Lafaysse, M., Berthier, E., Fanise, P., and Gascoin, S.: Improving the Spatial Distribution of Snow Cover Simulations by Assimilation of Satellite Stereoscopic Imagery, Water Resources Research, 58, https://doi.org/10.1029/2021WR030271, 2022.

Deschamps-Berger, C., Gascoin, S., Shean, D., Besso, H., Guiot, A., and López-Moreno, J. I.: Evaluation of snow depth retrievals from ICESat-2 using airborne laser-scanning data, The Cryosphere, 17, 2779–2792, https://doi.org/10.5194/tc-17-2779-2023, 2023.

Dozier, J.: Mountain hydrology, snow color, and the fourth paradigm, EoS Transactions, 92, 373–374, https://doi.org/10.1029/2011EO430001, 2011.

Dozier, J., Bair, E. H., and Davis, R. E.: Estimating the spatial distribution of snow water equivalent in the world's mountains, WIREs Water, 3, 461–474, https://doi.org/10.1002/wat2.1140, 2016.

Dunmire, D., Lievens, H., Boeykens, L., and De Lannoy, G. J. M.: A machine learning approach for estimating snow depth across the European Alps from Sentinel-1 imagery, Remote Sensing of Environment, 314, 114369, https://doi.org/10.1016/j.rse.2024.114369, 2024.

Elder, K., Rosenthal, W., and Davis, R. E.: Estimating the spatial distribution of snow water equivalence in a montane watershed, Hydrol. Process., 12, 1793–1808, https://doi.org/10.1002/(SICI)1099-1085(199808/09)12:10/11<1793::AID-HYP695>3.0.CO;2-K, 1998.

Essery, R.: A factorial snowpack model (FSM 1.0), Geosci. Model Dev., 8, 3867–3876, https://doi.org/10.5194/gmd-8-3867-2015, 2015.

https://doi.org/10.5194/egusphere-2025-978
Preprint. Discussion started: 21 March 2025

599 Essery, R., Mazzotti, G., Barr, S., Jonas, T., Quaife, T., and Rutter, N.: A Flexible Snow Model
600 (FSM 2.1.0) including a forest canopy, https://doi.org/10.5194/egusphere-2024-2546, 11 October
601 2024.

602 Feldman, D. R., Aiken, A. C., Boos, W. R., Carroll, R. W. H., Chandrasekar, V., Collis, S.,
603 Creamean, J. M., De Boer, G., Deems, J., DeMott, P. J., Fan, J., Flores, A. N., Gochis, D.,
604 Grover, M., Hill, T. C. J., Hodshire, A., Hulm, E., Hume, C. C., Jackson, R., Junyent, F.,
605 Kennedy, A., Kumjian, M., Levin, E. J. T., Lundquist, J. D., O'Brien, J., Raleigh, M. S., Reithel,
606 J., Rhoades, A., Rittger, K., Rudisill, W., Sherman, Z., Siirila-Woodburn, E., Skiles, S. M., Smith,
607 J. N., Sullivan, R. C., Theisen, A., Tuftedal, M., Varble, A. C., Wiedlea, A., Wielandt, S.,
608 Williams, K., and Xu, Z.: The Surface Atmosphere Integrated Field Laboratory (SAIL)
609 Campaign, Bulletin of the American Meteorological Society, 104, E2192–E2222,
610 https://doi.org/10.1175/BAMS-D-22-0049.1, 2023.

611 Foster, J., Liston, G., Koster, R., Essery, R., Behr, H., Dumenil, L., Verseghy, D., Thompson, S.,
612 Pollard, D., and Cohen, J.: Snow Cover and Snow Mass Intercomparisons of General Circulation
613 Models and Remotely Sensed Datasets, J. Climate, 9, 409–426, https://doi.org/10.1175/1520-
614 0442(1996)009<0409:SCASMI>2.0.CO;2, 1996.

615 Gagliano, E., Shean, D., Henderson, S., and Vanderwilt, S.: Capturing the Onset of Mountain
616 Snowmelt Runoff Using Satellite Synthetic Aperture Radar, Geophysical Research Letters, 50,
617 e2023GL105303, https://doi.org/10.1029/2023GL105303, 2023.

618 Girotto, M., Musselman, K. N., and Essery, R. L. H.: Data Assimilation Improves Estimates of
619 Climate-Sensitive Seasonal Snow, Curr Clim Change Rep, 6, 81–94,
620 https://doi.org/10.1007/s40641-020-00159-7, 2020.

621 Girotto, M., Formetta, G., Azimi, S., Bachand, C., Cowherd, M., De Lannoy, G., Lievens, H.,
622 Modanesi, S., Raleigh, M. S., Rigon, R., and Massari, C.: Identifying snowfall elevation patterns
623 by assimilating satellite-based snow depth retrievals, Science of The Total Environment, 906,
624 167312, https://doi.org/10.1016/j.scitotenv.2023.167312, 2024.

625 Grünewald, T., Schirmer, M., Mott, R., and Lehning, M.: Spatial and temporal variability of
626 snow depth and ablation rates in a small mountain catchment, The Cryosphere, 4, 215–225,
627 https://doi.org/10.5194/tc-4-215-2010, 2010.

628 Herbert, J. N., Raleigh, M. S., and Small, E. E.: Reanalyzing the spatial representativeness of
629 snow depth at automated monitoring stations using airborne lidar data, The Cryosphere, 18,
630 3495–3512, https://doi.org/10.5194/tc-18-3495-2024, 2024.

631 Hersbach, H., Bell, B., Berrisford, P., Hirahara, S., Horányi, A., Muñoz-Sabater, J., Nicolas, J.,
632 Peubey, C., Radu, R., Schepers, D., Simmons, A., Soci, C., Abdalla, S., Abellan, X., Balsamo,
633 G., Bechtold, P., Biavati, G., Bidlot, J., Bonavita, M., De Chiara, G., Dahlgren, P., Dee, D.,
634 Diamantakis, M., Dragani, R., Flemming, J., Forbes, R., Fuentes, M., Geer, A., Haimberger, L.,
635 Healy, S., Hogan, R. J., Hólm, E., Janisková, M., Keeley, S., Laloyaux, P., Lopez, P., Lupu, C.,
636 Radnoti, G., De Rosnay, P., Rozum, I., Vamborg, F., Villaume, S., and Thépaut, J.: The ERA5
637 global reanalysis, Quart J Royal Meteoro Soc, 146, 1999–2049, https://doi.org/10.1002/qj.3803,
638 2020.

https://doi.org/10.5194/egusphere-2025-978
Preprint. Discussion started: 21 March 2025

Hoppinen, Z., Palomaki, R. T., Brencher, G., Dunmire, D., Gagliano, E., Marziliano, A., Tarricone, J., and Marshall, H.-P.: Evaluating snow depth retrievals from Sentinel-1 volume scattering over NASA SnowEx sites, The Cryosphere, 18, 5407–5430, https://doi.org/10.5194/tc-18-5407-2024, 2024.

Hu, Y., Lu, X., Zeng, X., Stamnes, S. A., Neuman, T. A., Kurtz, N. T., Zhai, P., Gao, M., Sun, W., Xu, K., Liu, Z., Omar, A. H., Baize, R. R., Rogers, L. J., Mitchell, B. O., Stamnes, K., Huang, Y., Chen, N., Weimer, C., Lee, J., and Fair, Z.: Deriving Snow Depth From ICESat-2 Lidar Multiple Scattering Measurements, Front. Remote Sens., 3, 855159, https://doi.org/10.3389/frsen.2022.855159, 2022.

Hubbard, S. S., Williams, K. H., Agarwal, D., Banfield, J., Beller, H., Bouskill, N., Brodie, E., Carroll, R., Dafflon, B., Dwivedi, D., Falco, N., Faybishenko, B., Maxwell, R., Nico, P., Steefel, C., Steltzer, H., Tokunaga, T., Tran, P. A., Wainwright, H., and Varadharajan, C.: The East River, Colorado, Watershed: A Mountainous Community Testbed for Improving Predictive Understanding of Multiscale Hydrological–Biogeochemical Dynamics, Vadose Zone Journal, 17, 1–25, https://doi.org/10.2136/vzj2018.03.0061, 2018.

Kelly, R. E., Chang, A. T., Tsang, L., and Foster, J. L.: A prototype AMSR-E global snow area and snow depth algorithm, IEEE Trans. Geosci. Remote Sensing, 41, 230–242, https://doi.org/10.1109/TGRS.2003.809118, 2003.

Kinar, N. J. and Pomeroy, J. W.: Measurement of the physical properties of the snowpack, Reviews of Geophysics, 53, 481–544, https://doi.org/10.1002/2015RG000481, 2015.

Largeron, C., Dumont, M., Morin, S., Boone, A., Lafaysse, M., Metref, S., Cosme, E., Jonas, T., Winstral, A., and Margulis, S. A.: Toward Snow Cover Estimation in Mountainous Areas Using Modern Data Assimilation Methods: A Review, Front. Earth Sci., 8, 325, https://doi.org/10.3389/feart.2020.00325, 2020.

Lievens, H., Demuzere, M., Marshall, H.-P., Reichle, R. H., Brucker, L., Brangers, I., De Rosnay, P., Dumont, M., Girotto, M., Immerzeel, W. W., Jonas, T., Kim, E. J., Koch, I., Marty, C., Saloranta, T., Schöber, J., and De Lannoy, G. J. M.: Snow depth variability in the Northern Hemisphere mountains observed from space, Nat Commun, 10, 4629, https://doi.org/10.1038/s41467-019-12566-y, 2019.

Lievens, H., Brangers, I., Marshall, H.-P., Jonas, T., Olefs, M., and De Lannoy, G.: Sentinel-1 snow depth retrieval at sub-kilometer resolution over the European Alps, The Cryosphere, 16, 159–177, https://doi.org/10.5194/tc-16-159-2022, 2022.

López-Moreno, J. I., Fassnacht, S. R., Beguería, S., and Latron, J. B. P.: Variability of snow depth at the plot scale: implications for mean depth estimation and sampling strategies, The Cryosphere, 5, 617–629, https://doi.org/10.5194/tc-5-617-2011, 2011.

Lundquist, J. D., Kim, R. S., Durand, M., and Prugh, L. R.: Seasonal Peak Snow Predictability Derived From Early-Season Snow in North America, Geophysical Research Letters, 50, e2023GL103802, https://doi.org/10.1029/2023GL103802, 2023.

https://doi.org/10.5194/egusphere-2025-978
Preprint. Discussion started: 21 March 2025

Luojus, K., Pulliainen, J., Takala, M., Lemmetyinen, J., Mortimer, C., Derksen, C., Mudryk, L., Moisander, M., Hiltunen, M., Smolander, T., Ikonen, J., Cohen, J., Salminen, M., Norberg, J., Veijola, K., and Venäläinen, P.: GlobSnow v3.0 Northern Hemisphere snow water equivalent dataset, Sci Data, 8, 163, https://doi.org/10.1038/s41597-021-00939-2, 2021.

Margulis, S. A., Girotto, M., Cortés, G., and Durand, M.: A Particle Batch Smoother Approach to Snow Water Equivalent Estimation, Journal of Hydrometeorology, 16, 1752–1772, https://doi.org/10.1175/JHM-D-14-0177.1, 2015.

Margulis, S. A., Fang, Y., Li, D., Lettenmaier, D. P., and Andreadis, K.: The Utility of Infrequent Snow Depth Images for Deriving Continuous Space-Time Estimates of Seasonal Snow Water Equivalent, Geophysical Research Letters, 46, 5331–5340, https://doi.org/10.1029/2019GL082507, 2019.

Marti, R., Gascoin, S., Berthier, E., De Pinel, M., Houet, T., and Laffly, D.: Mapping snow depth in open alpine terrain from stereo satellite imagery, The Cryosphere, 10, 1361–1380, https://doi.org/10.5194/tc-10-1361-2016, 2016.

Mazzolini, M., Aalstad, K., Alonso-González, E., Westermann, S., and Treichler, D.: Spatio-temporal snow data assimilation with the ICESat-2 laser altimeter, https://doi.org/10.5194/egusphere-2024-1404, 24 May 2024.

McGrath, D., Webb, R., Shean, D., Bonnell, R., Marshall, H., Painter, T. H., Molotch, N. P., Elder, K., Hiemstra, C., and Brucker, L.: Spatially Extensive Ground-Penetrating Radar Snow Depth Observations During NASA's 2017 SnowEx Campaign: Comparison With In Situ, Airborne, and Satellite Observations, Water Resources Research, 55, 10026–10036, https://doi.org/10.1029/2019WR024907, 2019.

Molotch, N. P. and Bales, R. C.: SNOTEL representativeness in the Rio Grande headwaters on the basis of physiographics and remotely sensed snow cover persistence, Hydrological Processes, 20, 723–739, https://doi.org/10.1002/hyp.6128, 2006.

Nagler, T., Rott, H., Ripper, E., Bippus, G., and Hetzenecker, M.: Advancements for Snowmelt Monitoring by Means of Sentinel-1 SAR, Remote Sensing, 8, 348, https://doi.org/10.3390/rs8040348, 2016.

Oveisgharan, S., Zinke, R., Hoppinen, Z., and Marshall, H. P.: Snow water equivalent retrieval over Idaho – Part 1: Using Sentinel-1 repeat-pass interferometry, The Cryosphere, 2024.

Painter, T. H., Berisford, D. F., Boardman, J. W., Bormann, K. J., Deems, J. S., Gehrke, F., Hedrick, A., Joyce, M., Laidlaw, R., Marks, D., Mattmann, C., McGurk, B., Ramirez, P., Richardson, M., Skiles, S. M., Seidel, F. C., and Winstral, A.: The Airborne Snow Observatory: Fusion of scanning lidar, imaging spectrometer, and physically-based modeling for mapping snow water equivalent and snow albedo, Remote Sensing of Environment, 184, 139–152, https://doi.org/10.1016/j.rse.2016.06.018, 2016.

https://doi.org/10.5194/egusphere-2025-978
Preprint. Discussion started: 21 March 2025

Raleigh, M. S. and Small, E. E.: Snowpack density modeling is the primary source of uncertainty when mapping basin-wide SWE with lidar, Geophysical Research Letters, 44, 3700–3709, https://doi.org/10.1002/2016GL071999, 2017.

Rittger, K., Bair, E. H., Kahl, A., and Dozier, J.: Spatial estimates of snow water equivalent from reconstruction, Advances in Water Resources, 94, 345–363, https://doi.org/10.1016/j.advwatres.2016.05.015, 2016.

Smyth, E. J., Raleigh, M. S., and Small, E. E.: Particle Filter Data Assimilation of Monthly Snow Depth Observations Improves Estimation of Snow Density and SWE, Water Resources Research, 55, 1296–1311, https://doi.org/10.1029/2018WR023400, 2019.

Smyth, E. J., Raleigh, M. S., and Small, E. E.: Improving SWE Estimation With Data Assimilation: The Influence of Snow Depth Observation Timing and Uncertainty, Water Resources Research, 56, https://doi.org/10.1029/2019WR026853, 2020.

Smyth, E. J., Raleigh, M. S., and Small, E. E.: The Challenges of Simulating SWE Beneath Forest Canopies are Reduced by Data Assimilation of Snow Depth, Water Resources Research, 58, e2021WR030563, https://doi.org/10.1029/2021WR030563, 2022.

Sourp, L., Gascoin, S., Jarlan, L., Pedinotti, V., Bormann, K. J., and Baba, M. W.: Evaluation of high-resolution snowpack simulations from global datasets and comparison with Sentinel-1 snow depth retrievals in the Sierra Nevada, USA, Hydrol. Earth Syst. Sci., 29, 597–611, https://doi.org/10.5194/hess-29-597-2025, 2025.

Sturm, M. and Liston, G. E.: Revisiting the Global Seasonal Snow Classification: An Updated Dataset for Earth System Applications, Journal of Hydrometeorology, https://doi.org/10.1175/JHM-D-21-0070.1, 2021.

Treichler, D. and Kääb, A.: Snow depth from ICESat laser altimetry — A test study in southern Norway, Remote Sensing of Environment, 191, 389–401, https://doi.org/10.1016/j.rse.2017.01.022, 2017.

USDA,NRCS: SNOTEL Data, 2024.